

## Transient, Seasonal and Interannual Variability of the Taiwan Strait Current

CHAU-RON WU<sup>1\*</sup>, SHENN-YU CHAO<sup>2</sup> and CHUN HSU<sup>1</sup>

<sup>1</sup>Department of Earth Sciences, National Taiwan Normal University, Taipei 116, Taiwan, ROC

<sup>2</sup>Horn Point Laboratory, University of Maryland Center for Environmental Science, Cambridge, MD 21613, U.S.A.

(Received 18 July 2006; in revised form 14 May 2007; accepted 14 May 2007)

We have constructed a fine-resolution model with realistic bathymetry to study the spatial and temporal variations of circulation in the Taiwan Strait (TS). The TS model with a resolution of 3~10 km derives its open boundary conditions from a larger-scale model. The QSCAT/NCEP winds and AVHRR SST provide forcing at the sea surface. Because of the high resolution in model grids and forcing, the model achieves a previously unavailable level of agreement with most observations. On biweekly time scales surface-trapped current reversals often lead to Strait transport reversals if the northeasterly wind bursts in winter are sufficiently strong. On seasonal time scales the northward current is the strongest in summer since both summer monsoon and pressure gradient force are northward. The summer northward current appears to be relatively unimpeded by the Changyun Rise (CYR) and bifurcates slightly near the surface. With the arrival of the northeast monsoon in fall, downwind movement of China Coastal Water (CCW) is blocked by the northward current near 25.5°N and 120°E. In winter, the northward current weakens even more as the northeasterly monsoon strengthens. The CCW moves downwind along the western boundary; the CYR blocks part of the CCW and forces a U-shaped flow pattern in the northern Strait. Past studies have failed to reveal an anticyclonic eddy that develops on the northern flank of CYR in winter. On interannual time scales a weakened northeast monsoon during El Niño reduces advection of the cold CCW from the north and enhances intrusion of warm water from the south, resulting in warming in the TS.

Keywords:

- Taiwan Strait circulation,
- El Niño effect on Taiwan Strait,
- monsoon effect on Taiwan Strait.

### 1. Introduction

The Taiwan Strait is a narrow passage connecting the broad and shallow East China Sea to the much deeper South China Sea. The Strait is generally shallower than 60 m except over the deep Penghu Channel in the south-eastern corner (Fig. 1(a)). On seasonal time scales, monsoonal winds, southwesterly in summer and northeasterly in other seasons, drive part of the Strait circulation. The wind speed is generally weak in summer but becomes much stronger during winter. Beyond the seasonal time scale, interannual wind fluctuations related to El Niño/Southern Oscillation (ENSO) are also evident. In a four-year period from April 1996 to December 2000, winds during the 1997/1998 El Niño were relatively weaker; the much weakened northeasterly wind during

the 1997/1998 El Niño winter led to warmer sea surface temperature (SST) in the Strait, as revealed by satellite images (Kuo and Ho, 2004).

Circulation through the Taiwan Strait plays a crucial role in the material transport and nutrient budget in the East China Sea. Unfortunately, direct, long-term measurements of currents are often unavailable due to intense fishing pressure. Short-term current measurements have shed some light on the circulation in the Strait. For example, a point measurement deep in the Penghu Channel from March to October, 1984, revealed a mean northward current with occasional flow reversals, even though the prevailing wind was southward (Chuang, 1985). Later, shipboard acoustic Doppler current profiler (ADCP) observations collected between 1990 and 2001 (Liang *et al.*, 2003) confirmed the generally northward currents. Continuous velocity observations obtained from bottom-mounted ADCPs from October to November 1999 further demonstrated that the along-strait current was gen-

\* Corresponding author. E-mail: cwu@ntnu.edu.tw

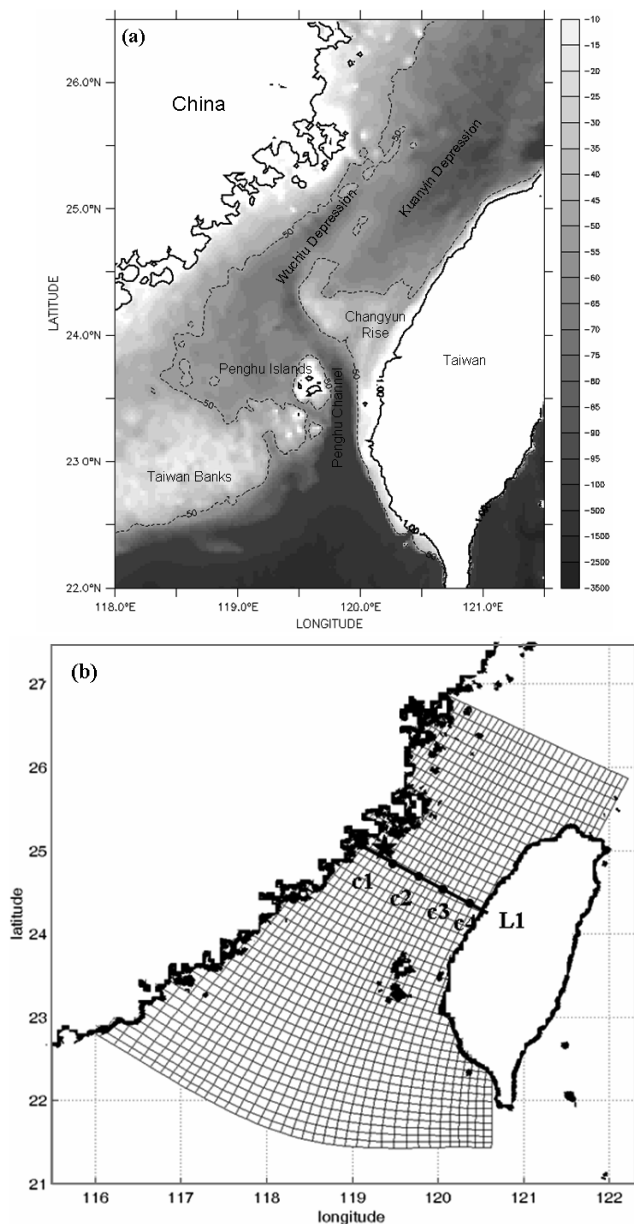


Fig. 1. (a) Taiwan Strait with realistic bathymetry. (b) Orthogonal curvilinear grid and locations of four ADCP mooring stations.

erally against the wind when the northeast wind was weak. However, during strong northeasterly wind bursts, strong southwestward flow could occur, bringing the cold China Coastal Water southward (Lin *et al.*, 2005).

Three-dimensional numerical modeling efforts have been improving recently. The early model (Jan *et al.*, 2002) was process-oriented, using monthly mean wind and monthly inflow-outflow to drive the Strait circulation. Events above and below the seasonal time scale were

truncated. A real-time, North Pacific Ocean, data-assimilating model (Ko *et al.*, 2003) examined local-versus-remote wind influence on the observed Strait transport reversals during October and November 1999; emphasis is on transport reversals rather than the Strait circulation itself. A  $1/8^\circ$  resolution hindcast model (Wu and Hsin, 2005) reexamined the Strait volume transport. When compared to estimates made by historical bottom-mounted ADCP and shipboard ADCP observations, the model revealed previous biases in transport estimates caused by the lack of winter measurements, and identified the QSCAT/NCEP (NASA Quick Scatterometer/NCEP) data set as the optimum wind forcing to drive the Strait circulation.

Even more recently, intensive observations have revealed new mesoscale, event-like and interannual features that are beyond the resolution and explanatory ability of previous models. These new findings call for renewed modeling efforts with much better resolution. In the present paper we improve the model of Wu and Hsin (2005) by refining bathymetry and forcing with a higher horizontal resolution ranging from 3 to 10 km, bringing the model skill to a level capable of coping with recent observations. Since the improved Taiwan Strait model resolves temporal and spatial scales of interest, we use the results to discuss the transient, seasonal and interannual variations.

## 2. Model Description

The Taiwan Strait (TS) model is formulated on the basis of the sigma-coordinate Princeton Ocean Model (POM; Blumberg and Mellor, 1987). The three-dimensional model solves the primitive equations for momentum, salt, and heat. It includes a 2.5-level turbulence closure sub-model developed by Mellor and Yamada (1982), and the Smagorinsky (1963) formulation for horizontal mixing. Figure 1(b) shows the orthogonal, curvilinear grid system and model domain. The horizontal grid size varies from 3 to 10 km, with finer resolution located near the center of the Strait. The model has 26 vertical sigma levels. On open boundaries, the TS model derives its boundary condition from a larger-scale East Asian Marginal Seas (EAMS) model, which also adopts the POM formulation with a horizontal resolution of  $1/8^\circ$  and 26 sigma levels. The EAMS model domain extends from  $99^\circ\text{E}$  to  $140^\circ\text{E}$  in longitude, and from  $0^\circ\text{N}$  to  $42^\circ\text{N}$  in latitude. A detailed description of the EAMS model has been given by Wu and Hsin (2005). The EAMS model has been validated with observed temperature and salinity data in the South China Sea and corroborated with observed velocity data from both bottom-mounted and shipboard ADCPs in the Taiwan Strait.

The POM uses the mode splitting technique to solve the depth-integrated governing equations (barotropic,

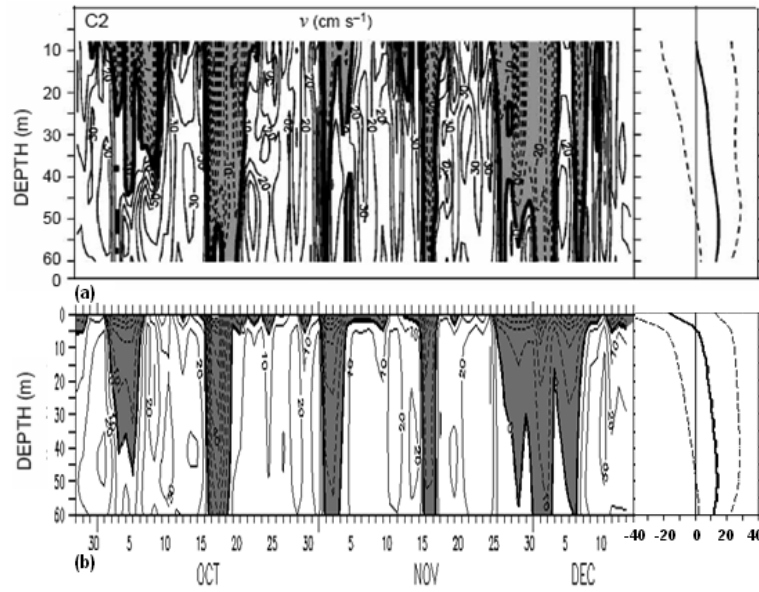


Fig. 2. 36-hour, low-pass filtered time series of along-strait current profiles at C2 calculated from (a) bottom-mounted ADCP (after Lin *et al.*, 2005), and (b) model simulation. Contour interval is 10 cm/s. Shading and dashed contours indicate southward currents. Right panels show vertical distributions of the mean current and its standard deviation.

external mode) and the equations governing vertical structure (baroclinic, internal mode) separately. The one-way coupling between the TS and EAMS models is as follows. Following Flather (1976), the vertically averaged velocity on open boundaries of the TS model is

$$\bar{u}_n = \bar{u}_n^0 + \sqrt{\frac{g}{H}}(\eta - \eta^0), \quad (1)$$

where  $\bar{u}_n$  is the depth-averaged velocity normal to open boundaries of the TS model at time  $t$  and  $\bar{u}_n^0$  is the corresponding velocity at time  $t$ , estimated from the EAMS model. The model sea surface height  $\eta$  is located half of a grid inside the open boundary in the TS model domain. The EAMS model sea surface height  $\eta^0$  is located on the open boundary of the TS model. The water depth on the open boundary is  $H$ , and  $g$  is the gravitational acceleration. Further, the zero normal gradient condition for sea level is used on all open boundaries. Baroclinic velocities on open boundaries of the TS model are determined using an inflow condition; daily baroclinic velocities from the EAMS model are spatially interpolated and assigned to the open boundary grids of the TS model. Temperature and salinity on the open boundaries are subject to upstream advection and, in case of inflow, daily EAMS profiles of temperature and salinity supply the upstream values.

The TS model was initialized with the temperature

and salinity fields of the EAMS model outputs in January 1999 and thereafter subject to climatological forcing for one year. After the spin-up period, the TS model was forced with QSCAT/NCEP wind data sets. Having a temporal resolution of 6 hours and a spatial resolution of  $0.5^\circ \times 0.5^\circ$ , the blended QSCAT/NCEP wind stress data set is one of the most up-to-date, high-resolution datasets of ocean surface winds at the present time. We adopted six-hourly fields of zonal and meridional wind components 10 m above sea level with a resolution of  $0.5^\circ \times 0.5^\circ$ . These fields are derived from a space and time blend of QSCAT-DIRTH satellite scatterometer observations and NCEP analyses (Milliff *et al.*, 1999). The TS model was subject to six-hourly wind stress at the sea surface and open ocean boundary forcing (as described above) provided by the EAMS model. The AVHRR sea surface temperature is specified at the sea surface. The simulation period is from 1999 to 2003.

### 3. Results and Discussions

#### 3.1 Model experiments and validation

Observations of the current velocities in the Taiwan Strait are rare. Lin *et al.* (2005) presented the only strait-wide current velocity profiles available to date. From September 28 to December 14 of 1999, current velocity across the Taiwan Strait was measured by four bottom-mounted ADCPs (C1, C2, C3 and C4 in Fig. 1(b)). These observations are used below for model validation. Near

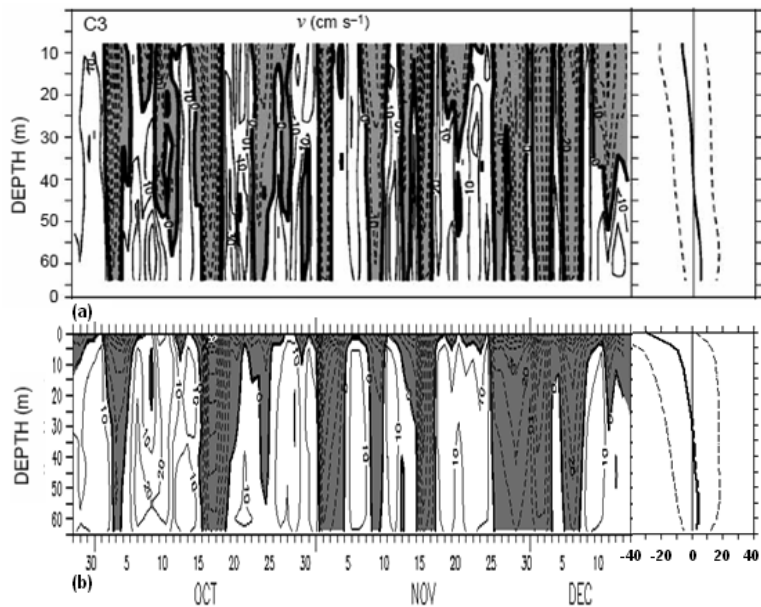


Fig. 3. As Fig. 2 but for C3.

the center of the Strait, a subsurface northward jet is often observed at C2. Figure 2(a), from Lin *et al.* (2005), shows the 36-hour, low-pass filtered time series of the along-strait current profile at C2, with its temporal mean and standard deviation in the right panel. The time averaging was over the entire duration of deployment. The time series in Fig. 2(a) shows velocity reversals at bi-weekly intervals, possibly caused by the passage of bi-weekly atmospheric winter fronts. Figure 2(b) shows corresponding results derived from the model. The observed and modeled velocity fluctuations agree not only in magnitude but also in phase. In particular, the model reproduced similar velocity reversals to those revealed by the observations. Below 8 m depth, the mean and standard deviation of the model-derived velocity in Fig. 2(b) are also in agreement with observations. Leaving the surface layer aside, the mean is positive (northward) and increases with depth; the standard deviations of both modeled and observed velocities decrease with depth, indicating smaller fluctuations deep in the water column. Additionally, the modeled velocity shows a downwind (southward) surface flow in the surface layer (shallower than 8 m) where no mooring data were available.

Figure 3 shows a similar model-data comparison at station C3. Relative to station C2, currents at station C3 are generally weaker but also exhibit similar biweekly reversals. Again, the model results (Fig. 3(b)) reproduce most of the observed trends in currents (Fig. 3(a)), including the magnitude and five reversal events. At C3, both the mooring data and model show a southward mean current in the upper layer and a northward mean current

in the lower layer. Additionally, the modeled mean current profile (Fig. 3(b)) shows a large southward speed near the surface where no mooring data were available.

Figure 4 shows a similar model-data comparison at the two nearshore stations, C1 and C4. The agreement at station C4 is again satisfactory. Station C1 is too close to irregular China coastlines and several islets. Our model resolution, although vastly improved, does not resolve the complex local bathymetry well and may therefore have missed some local flow disturbances. In consequence, the modeled velocities deviate somewhat from observations in terms of their magnitude. Nevertheless, the model captures major features at station C1.

The passage of biweekly atmospheric winter fronts is apparently responsible for velocity reversals. Figure 5 shows sequential zonal sections of model-derived, along-strait velocity distribution. An additional top panel shows 36-hour low-pass filtered time series of along-strait wind velocities that also delineate three episodes of strong northeasterly wind bursts. Below the wind time series, each column of zonal sections in Fig. 5 shows the ocean's response prior to, during, and shortly after each northeasterly wind burst. The duration of each wind event varied from 5 to 8 days, but the ocean's response was similar. Prior to each wind burst the along-strait velocity was generally northward, containing two cores, one near the center of the Strait and another off the west coast of Taiwan. As the northeast wind peaked, the along-strait velocity became mostly southward, further confirming the flow reversal during periods of strong northeasterly wind (Wu and Hsin, 2005). In the deepest reaches, the north-

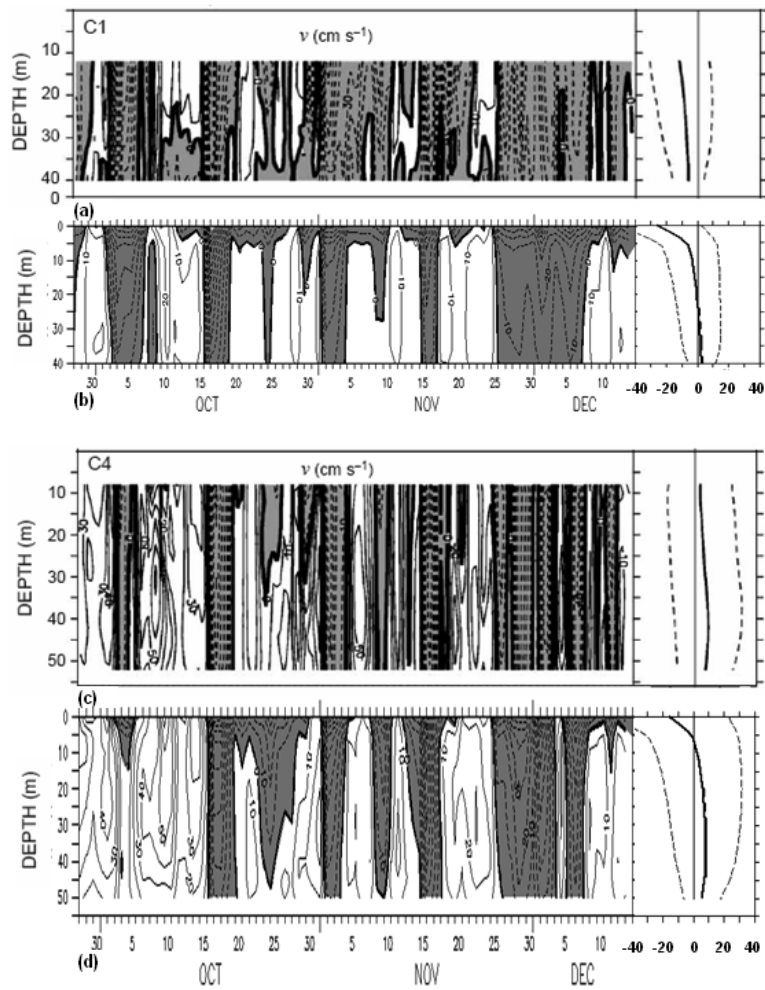


Fig. 4. As Fig. 2 but for C1 and C4.

ward current persists against the strong wind. The down-wind current distribution is not uniform across the Strait; bottom topography and temperature variations could cause the uneven distribution. During relaxation of the strong northeasterly wind, the northward undercurrent expanded upward at the expense of the southward current, returning to the pre-wind condition over time. The observed current structures (figure 13 in Lin *et al.*, 2005) were similar, except for a slightly faster development of the relaxation phase.

Figure 6 shows the model-derived Strait transport across the Taiwan Strait from October to November 1999 together with the observation-based estimate (from Ko *et al.*, 2003). The agreement is reasonable. For example, both transports reached around  $-5$  Sv (southward) on October 17, 1999. The present model result is also consistent with the report by Wu and Hsin (2005), who revealed net southward transport during strong northeast monsoon winds.

Averaging over the entire period from October to November 1999, the mean volume transport is 0.11 Sv whereas the observation-based estimate varied from  $-5$  to 2 Sv with a mean value of  $0.12 \pm 0.33$  Sv (Lin *et al.*, 2005).

### 3.2 Seasonal variations

On daily time scales and beyond, Wu and Hsin (2005) established an empirical relationship between volume transport ( $T_T$  in units of Sv) and along-strait wind stress ( $\tau$  in units of  $\text{dyne cm}^{-2}$ ) as  $T_T = 1.06 \times \tau + 1.99$ . In other words, both wind stress and a northward pressure gradient force contribute to the strait-wide volume transport. On average, the pressure gradient force is northward because the sea surface is always lower at the north entrance of the Taiwan Strait (Wu and Hsin, 2005). This pressure gradient force drives a mean northward volume transport of 1.99 Sv all year round, independent of the winds. Since the Taiwan Strait is subject to strong monsoon forcing,

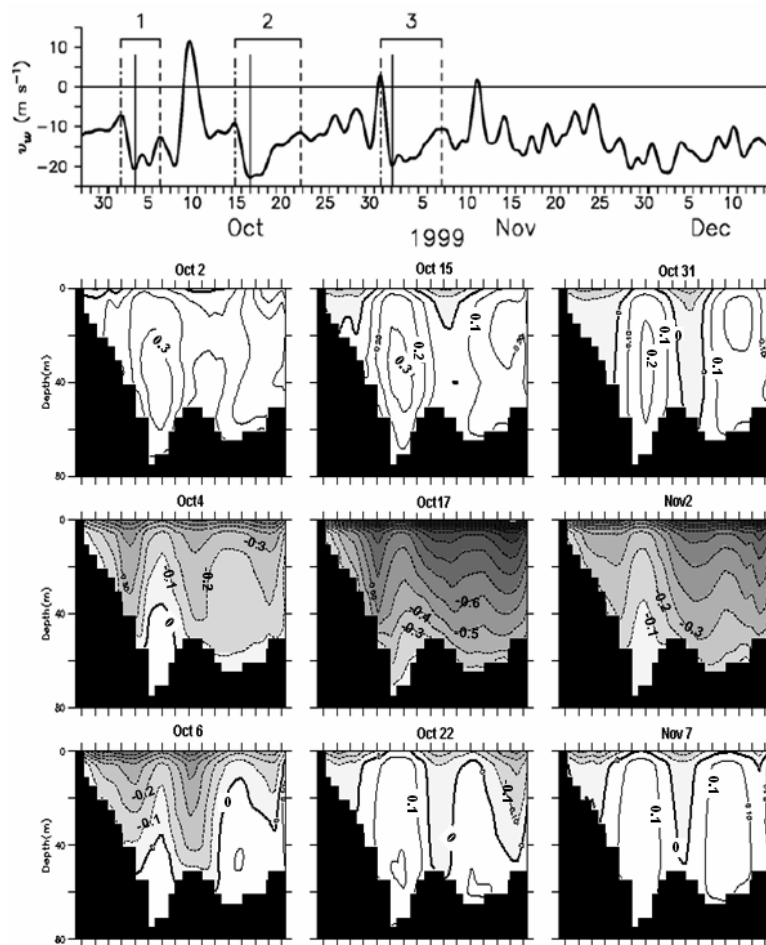


Fig. 5. Sequential cross-sections of the model-derived along-strait velocity along the four ADCP stations as shown in Fig. 1; view is northward. Additional top panel shows the time series of along-strait wind velocity and delineates three northeasterly wind burst events (after Lin *et al.*, 2005). Contour interval is 0.1 m/s. Solid and dashed contours are northward and southward currents, respectively, separated by the thick, zero-speed contours.

season is defined below according to the monsoon rather than the calendar. Further, although the salinity is not a passive tracer, temperature is the major indicator of water density and to a large degree determines the circulation inside the Taiwan Strait. We therefore use temperature field rather than salinity field below to facilitate the discussion.

#### Summer (June, July and August) circulation

Following the onset of the southwest monsoon over the Taiwan Strait in June, the winter circulation gradually enters the summer regime. The summer circulation peaks in August. Figures 7(a) and (b) show the summer circulation and temperature distribution at 20 m and 50 m, respectively. Since both summer monsoon and pressure gradient force are northward, the northward current is quite strong in summer. The northward current is the strongest in the Penghu Channel, the major pathway by which the northward flow enters the Taiwan Strait. The

northward current is relatively unimpeded by the Changyun Rise (CYR) and bifurcates slightly near surface. One branch continues northward over the CYR. Another branch moves around CYR along its western flank (Fig. 7(a)). The surface bifurcation also showed up in composite currents obtained from shipboard ADCPs between 1990 and 2001 (Liang *et al.*, 2003). The present model reproduces both the bifurcated path and current speed. Some of the northward currents from the South China Sea flow downwind along western reaches of the Strait. Temperature contours at 20 m roughly parallel the velocity vectors in the Strait, except in two cold anomalies north and southwest of the Penghu Islands. The cold core southwest of Penghu Islands coincides with a bottom topography rise while that north of Penghu Islands is over the southern flank of CYR. Shoaling bottom lifting of deeper water could conceivably produce upwelling in these two areas. Interestingly, cold anomalies around the

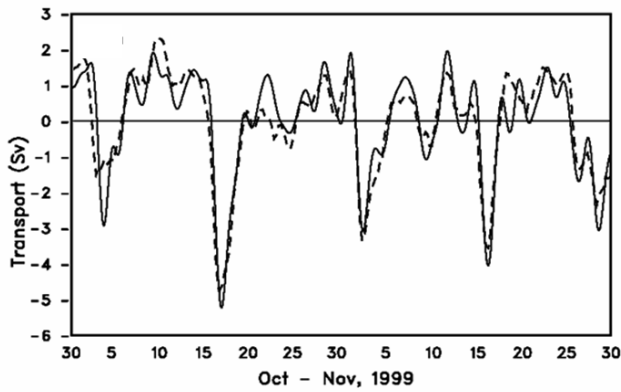


Fig. 6. Time series of model-derived volume transports across the Taiwan Strait from October to November 1999 (broken line) together with the observed transport (solid line, after Ko *et al.*, 2003).

Penghu Islands are frequently observed during summer (e.g. Wang and Chern, 1992; Hu *et al.*, 2003). Flow at 50 m depth (Fig. 7(b)) shows a similar pattern but without bifurcation, due to blockage by CYR.

#### Fall (September) circulation

Figure 8 shows the corresponding fall circulation and temperature distribution. The northward flow in fall becomes weaker with the arrival of the northeast monsoon. In particular, the northward intrusion current over and beyond the CYR shows a marked reduction in strength. Further, downwind acceleration allows the colder, fresher China Coastal Water to appear in the northwestern reaches of the Strait. The southward-flowing China Coastal Water is blocked by the northward current near 25.5°N and 120°E (Fig. 8(a)). Relative to summer, temperature is more uniform in fall. The cold anomaly north of the Penghu Islands still persists in fall (Fig. 8(a)). Excluding regions blocked by the shoaling bottom, a similar flow pattern exists at 50 m depth (Fig. 8(b)).

#### Winter (October, November, December, January and February) circulation

The development of the winter circulation continues from October to February of the following year. Driven by the northward pressure gradient force and northeasterly monsoon, the confluence of northward and southward currents complicates the circulation pattern (Fig. 9). Relative to fall, the northward current weakens even further as the prevailing northeasterly monsoon strengthens. The current is much weaker, being nearly stagnant in the Penghu Channel. The China Coastal Water moves downwind along the entire western boundary; part of it suffers blockage by the CYR in the middle reaches of Taiwan Strait, forming a U-shaped flow pattern that occupies the northern portion of the Strait. The U-turn causes the north-

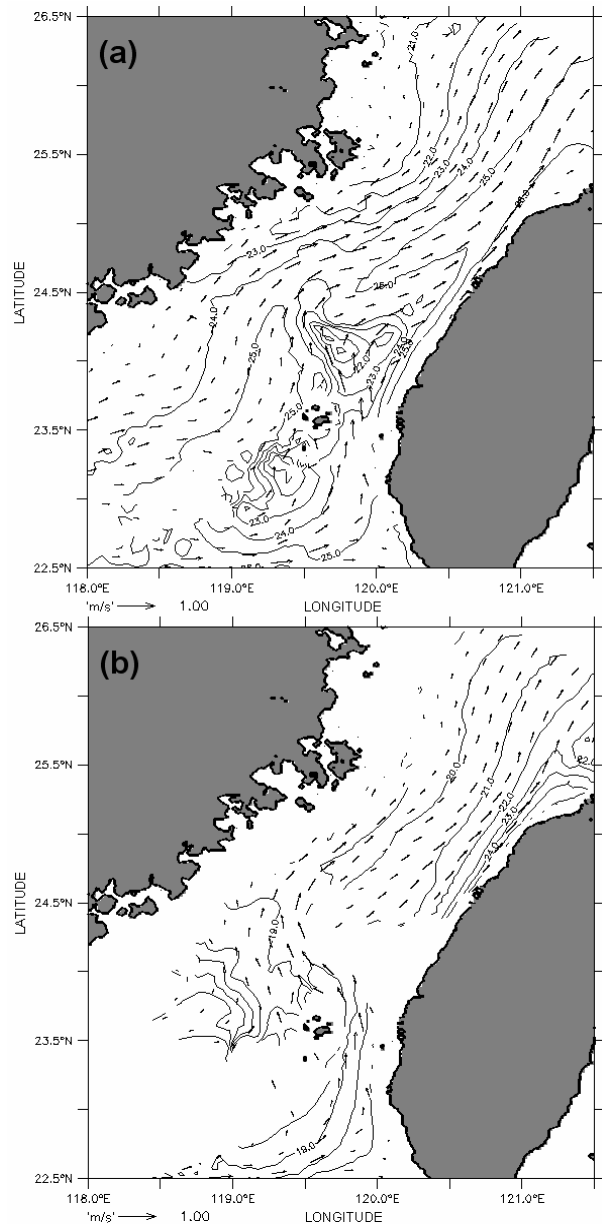


Fig. 7. Summer circulation and temperature distribution at (a) 20 m and (b) 50 m. Time averaging is over the period from June to August. Velocity scales are in m/s. Temperature contour interval is 1°C.

ern Strait water mass to differ substantially from the southern Strait water mass. A zonal oceanic front over the CYR sometimes exists in winter (e.g. Wang and Chern, 1988; Jan *et al.*, 2002; Li *et al.*, 2006). Temperature contours orient northeast-southwest in the northern portion of the Strait but gradually become zonal in the southern portion. After analyzing historical hydrographic data, Wang and Chern (1988) demonstrated that the southern water mass comes from Kuroshio Branch Water. Additionally,

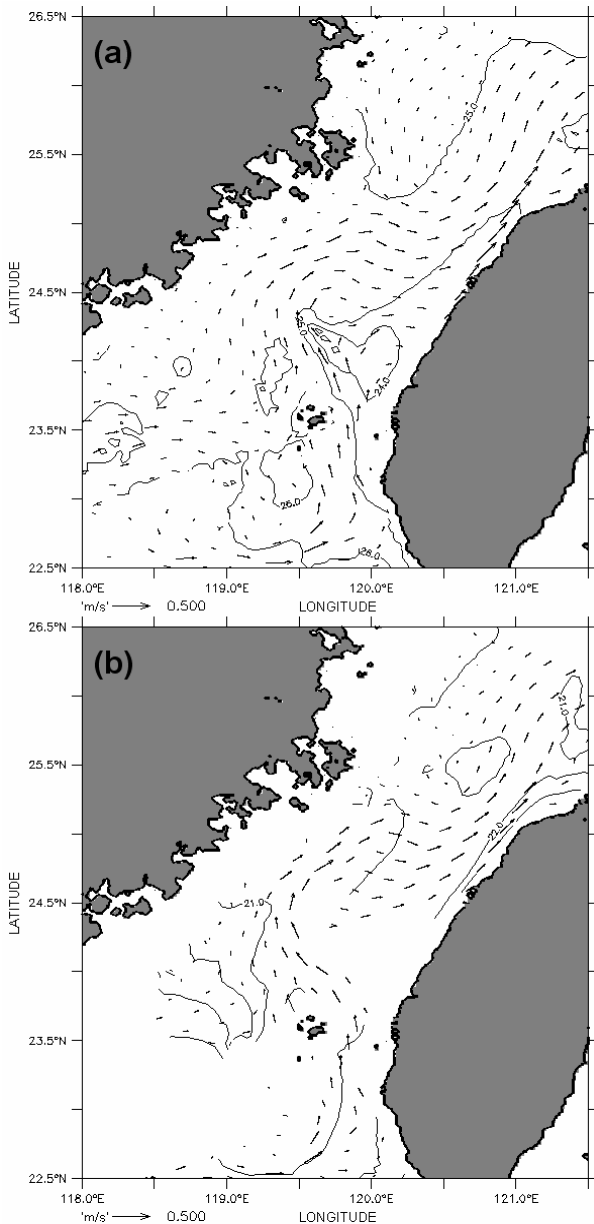


Fig. 8. Fall circulation and temperature distribution at (a) 20 m and (b) 50 m. Time averaging is over September. Velocity scales are in m/s. Temperature contour interval is 1°C.

Fig. 9(a) also shows the formation of an anticyclonic eddy in the central reaches of the Strait (over and slightly north of CYR). This appears to be a new feature, since previous models and historical data did not document such an eddy. Our improved model resolution is the key to produce the anticyclone. Historical data sets lacked winter observations and therefore cannot verify the anticyclone. However, recent winter current data measured by bottom-mounted ADCPs (Lin *et al.*, 2005) support the existence

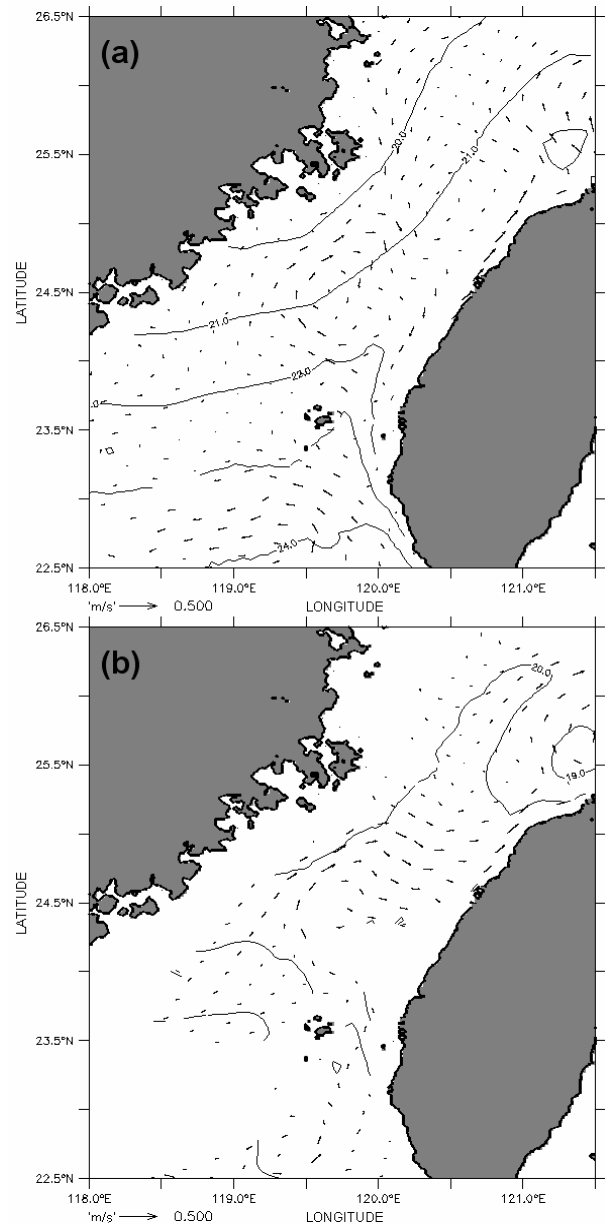


Fig. 9. Winter circulation and temperature distribution at (a) 20 m and (b) 50 m. Time averaging is over the period from October to February of the following year. Velocity scales are in m/s. Temperature contour interval is 1°C.

of such an anticyclone. The winter mean velocity in the upper ocean below the mixed layer is northward at station C2 (Fig. 2(a)) and southward at station C3 (Fig. 3(a)), lending some support to the existence of the anticyclone. Flow at 50 m depth is generally weaker and moves around CYR along its western flank (Fig. 9(b)).

The winter appearance of an anticyclone suggested by our model is also consistent with theoretical expecta-

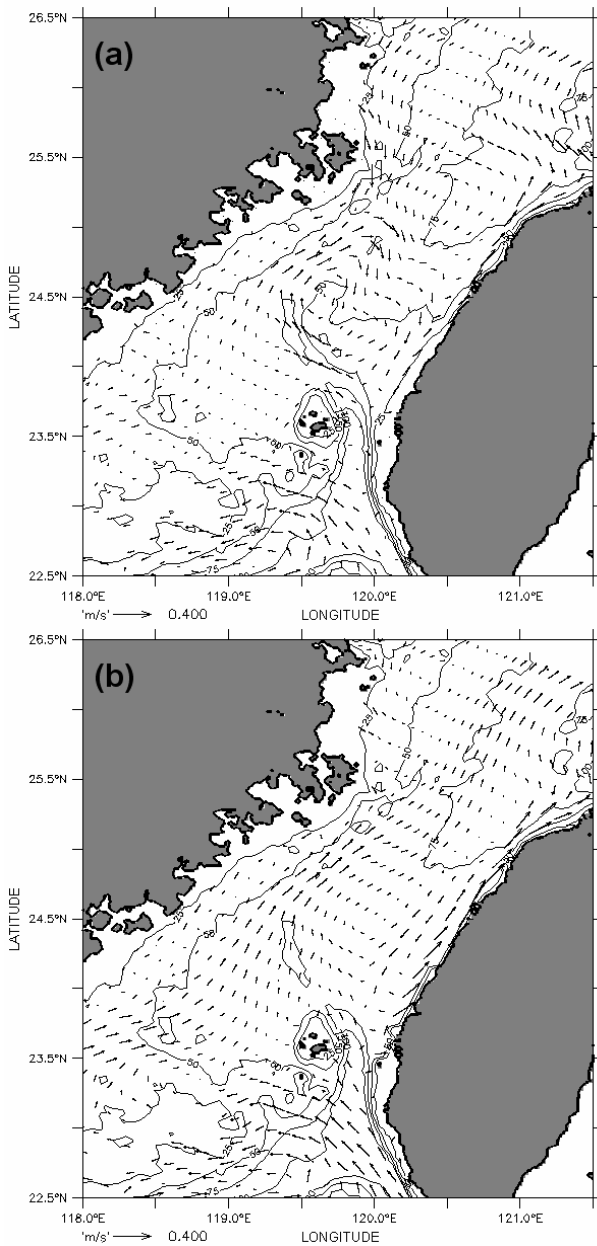


Fig. 10. Winter circulation patterns at 20 m and bottom depth contours (a) with realistic bottom topography and (b) after removing the CYR. Time averaging is over the period from October to February of the following year. Velocity scales are in m/s. Depth contour interval is 25 m.

tions. In homogeneous waters, flow over a seamount such as CYR will induce an anticyclone or Taylor column that extends from the bottom to the sea surface. Stratification will suppress the formation of the anticyclonic eddy (Hogg, 1973). Thus the winter destratification creates a better condition for the development of an anticyclone over CYR. To verify this, we repeated the simulation with

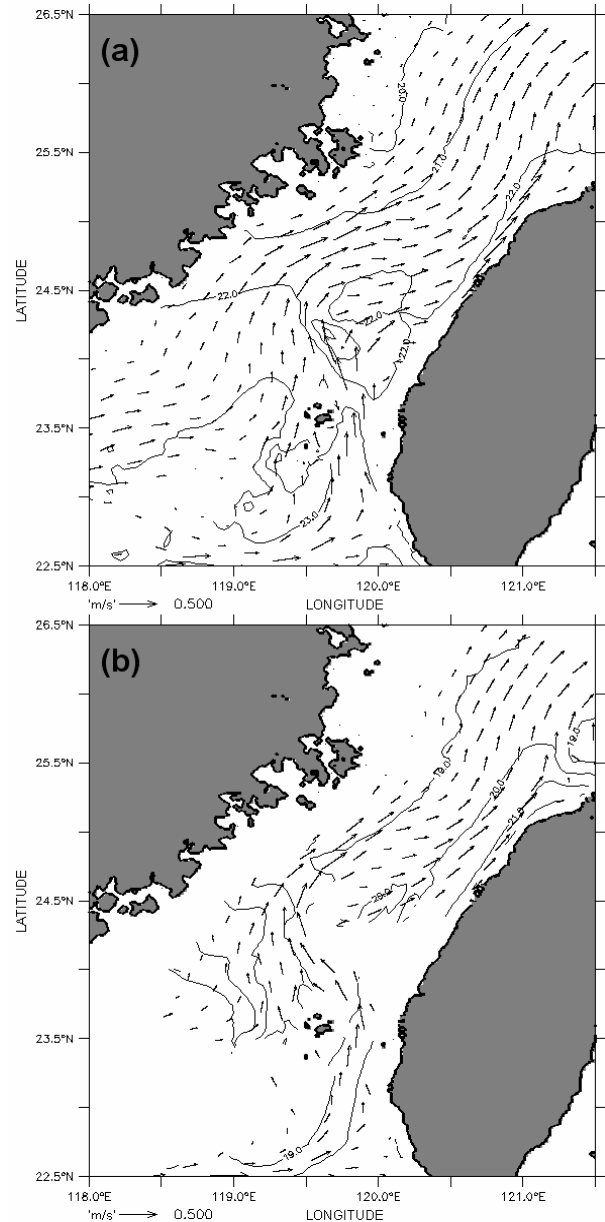


Fig. 11. Spring circulation and temperature distribution at (a) 20 m and (b) 50 m. Time averaging is over the period from March to May. Velocity scales are in m/s. Temperature contour interval is 1°C.

the CYR removed. Figure 10 compares mean winter flow fields at 20 m depth superimposed on bottom topography contours with and without CYR. With realistic topography, the anticyclonic eddy is well developed over and slightly north of CYR (Fig. 10(a)). The slight northward shift is conceivably due to northward advection. After removing CYR, the anticyclonic circulation is diffuse and unable to form a well-defined eddy (Fig. 10(b)).

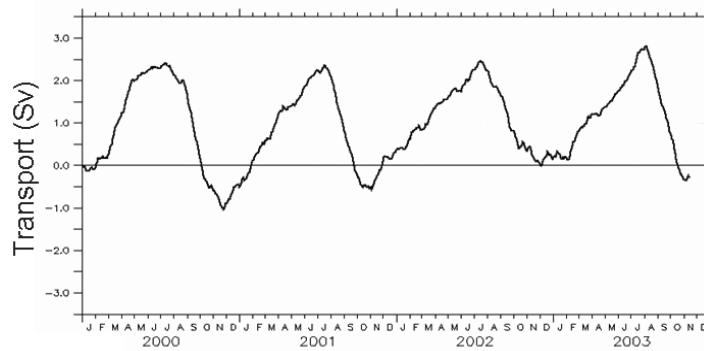


Fig. 12. Model-produced time series of 90-day running mean of volume transports through the Taiwan Strait from 2000 to 2003.

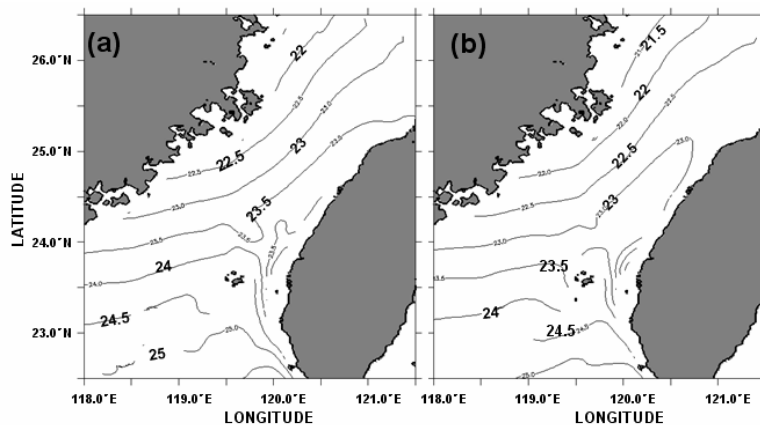


Fig. 13. Modeled monthly mean temperature at 20 m depth in (a) November 2002 and (b) November 2000.

### Spring (March, April and May) circulation

Figure 11 shows the spring circulation and temperature distribution at 20 m and 50 m. Relative to winter, the relaxation of the northeast monsoon during the spring transition reinvigorates the hitherto blocked northward current. The inflow from Penghu Channel strengthens and turns clockwise over the CYR. On the other hand, the southward-flowing China Coastal Water weakens. The circulation pattern (Fig. 11(a)) in spring resembles that in fall (Fig. 8(a)), but the temperature in spring is much lower than that in fall. Further, circulation in spring is fairly barotropic; surface and bottom features are quite similar. As summer approaches, the northward current strengthens further and will penetrate farther northward (Fig. 7), completing the annual cycle.

### 3.3 Interannual variability

Beyond seasonal variation, interannual variation also exists in the Strait. Figure 12 shows the 90-day running-mean of volume transport through the Taiwan Strait. The mean transport in summer 2003 is the largest in the four-

year period from 2000 to 2003. On the other hand, southward transport is smallest in winter of 2002 due to a weaker northeast monsoon (figure not shown). Apparently, ENSO is responsible for the interannual variability of the Strait transport.

In the four-year period, the Niño 3.4 SST index ( $5^{\circ}\text{S}$ – $5^{\circ}\text{N}$ ;  $170^{\circ}\text{W}$ – $120^{\circ}\text{W}$ ) peaked in November 2002 in response to an El Niño event in the tropical Pacific. On the other hand, the winter of 2000 was a La Niña episode, based on the criterion that the SST anomaly is less than  $-0.5^{\circ}\text{C}$  in the Niño 3.4 SST index. Figures 13(a) and (b) show the modeled monthly-mean temperature field at 20 m in November 2002 and November 2000, respectively. The temperature in the entire Strait was generally warmer in November 2002; the simulated results show warming of the upper ocean by  $0.5^{\circ}\text{C}$  during an El Niño winter. The tongue of the  $23.5^{\circ}\text{C}$  warm water from the Penghu Channel extended farther northward along the entire west coast of Taiwan in November 2002 (Fig. 13(a)), but stagnated around Penghu Islands in November 2000 (Fig. 13(b)). The colder ( $<22^{\circ}\text{C}$ ) water off the coast of China

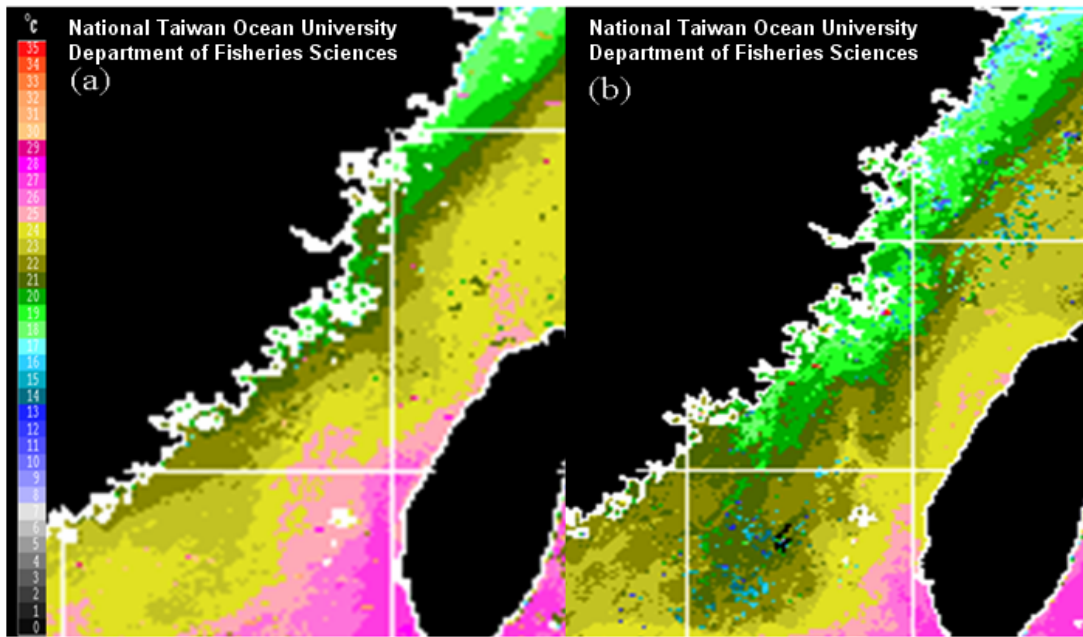


Fig. 14. Monthly-mean of NOAA/AVHRR SST images in (a) November 2002 and (b) November 2000 (from <http://www.ncor.ntu.edu.tw/>).

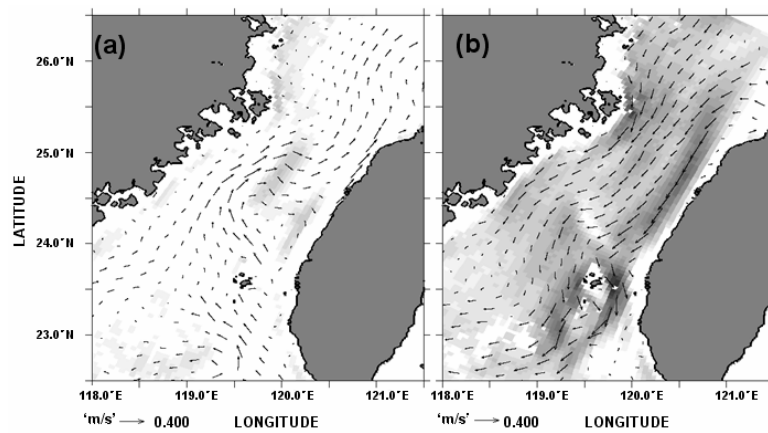


Fig. 15. Circulation at 20 m depth in (a) November 2002 and (b) November 2000. Velocity scales are in m/s. Shading indicates southward flow.

stretched as far south as 24.5°N in November 2000 (Fig. 13(b)), whereas it barely appeared in the northwestern tip of the Strait in November 2002 (Fig. 13(a)).

The monthly mean of NOAA/AVHRR SST images in November 2002 and November 2000 (Fig. 14) validates the model finding. Similar to Fig. 13, a nearly uniform northeast-southwest temperature gradient dominated the temperature field. Furthermore, in Fig. 14(a) the tongue of the 25°C warm water penetrated further north-

ward off the west coast of Taiwan in November 2002 (Fig. 14(a)), but stagnated south of Penghu Channel in November 2000 (Fig. 14(b)). Warming during an El Niño event in the Taiwan Strait has been observed in recent studies (e.g. Kuo and Ho, 2004; Shang *et al.*, 2005). For example, Shang *et al.* (2005) examined hydrographic and biological changes in the Taiwan Strait during the 1997/1998 El Niño winter using satellite images and field observations. They found a 25% increase in area covered by the

warm water and reduced concentrations of nutrients in the Strait during the 1997/1998 El Niño event. In the absence of observed currents, the anomalous warming calls for the following physical interpretation in terms of modeled circulation.

Figures 15(a) and (b) show modeled flow fields at 20 m depth in November 2002 and November 2000, respectively. A weakened northeast monsoon in November 2002 led to a much weaker downwind China Coastal Current that barely showed up in the northwestern tip of the Strait. On the other hand, the northward current, which is usually weak or absent during the normal winter, intruded along the Penghu Channel and thereafter the western flank of CYR (Fig. 15(a)). The reduced cold water intrusion from the north and enhanced warm water intrusion from the south resulted in warming in the Taiwan Strait in November 2002. On the other hand, with the aid of the anomalously strong northeast monsoon in November 2000, the southward-flowing China Coastal Water strengthened and occupied almost the entire Strait, while the northward intrusion current was absent (Fig. 15(b)). The predominance of southward advection led to water temperature decreases in the Taiwan Strait. The satellite images in Fig. 14 bear out the model finding.

#### 4. Concluding Remarks

This paper presents results from an observation-validated, three-dimensional model of the Taiwan Strait circulation. Improved spatial and temporal resolutions have revealed new features. Weather-band, seasonal and interannual variations show up quite realistically in this fine-resolution model. On weather-band time scales the model shows how biweekly passage of winter fronts modulates the Strait circulation. On seasonal time scales the combination of the monsoonal forcing and northward pressure gradient force modulate the Strait circulation. In summer these two forces reinforce each other, producing the strongest northward current; CYR exerts little impedance on the northward current and causes it to bifurcate slightly near the ocean surface. The model result not only lends support to the earlier description of summer circulation (Jan *et al.*, 2002), but also reveal new features, such as summer cold anomalies around Penghu Islands. With the arrival of the northeast monsoon in fall, downwind China Coastal Water is blocked by the northward current near 25.5°N and 120°E. In winter the northward current weakens even further as the prevailing northeasterly monsoon strengthens. The China Coastal Water moves downwind along the entire western boundary, but experiences partial blockage by CYR in the middle reaches of the Strait, forming a U-shaped flow pattern that occupies the northern reaches of the Strait. Thus, our model corroborates with the earlier description of winter circulation (Jan *et al.*, 2002) up to a point, beyond which

the present model suggests the existence of a winter anti-cyclonic eddy over and slightly north of CYR. The circulation pattern in spring is similar to that in fall.

Warming related to El Niño occurred in the winter of 2002, while the contemporaneous southward transport attained its minimum. Since the heat balance within the Taiwan Strait is determined in large part by inflows from north and south of the Strait, the modeled circulation is capable of explaining these warming events. A weakened northeast monsoon in the winter of 2002 reduced the southward intrusion of cold China Coastal Water and increased the northward intrusion of warm waters from the south, resulting in warming in the Strait. On the other hand, the strengthened winter monsoon during the La Niña event of 2000 strengthened the southward-flowing China Coastal Water but weakened or annihilated the northward current from the south; the colder China Coastal Water occupied almost the entire strait and decreased the water temperature in the Strait.

#### Acknowledgements

We would like to thank Dr. Atsuhiko Isobe of Kyushu University and two reviewers for suggestions. This research was supported by the National Science Council, Taiwan, ROC, under grants NSC 95-2611-M-003-001-MY3.

#### References

- Blumberg, A. F. and G. L. Mellor (1987): A description of a three-dimensional coastal ocean circulation model. p. 1–16. In *Coastal and Estuarine Sciences 4: Three Dimensional Coastal Models*, ed. by N. S. Heaps, AGU, Washington, D.C.
- Chuang, W.-S. (1985): Dynamics of subtidal flow in the Taiwan Strait. *J. Oceanogr. Soc. Japan*, **41**, 83–90.
- Flather, R. A. (1976): A tidal model of the north-west European continental shelf. *Memories de la Society Royal des Sciences de Liege*, **6**(10), 141–164.
- Hogg, N. G. (1973): On the stratified Taylor column. *J. Fluid Mech.*, **58**, 517–537.
- Hu, J., H. Kawamura, H. Hong and W. Pan (2003): A review of research on the upwelling in the Taiwan Strait. *Bull. Mar. Sci.*, **73**(3), 605–628.
- Jan, S., J. Wang, C.-S. Chern and S.-Y. Chao (2002): Seasonal variation of the circulation in the Taiwan Strait. *J. Mar. Sys.*, **35**, 249–268.
- Ko, D. S., R. H. Preller, G. A. Jacobs, T. Y. Tang and S. F. Lin (2003): Transport reversals at Taiwan Strait during October and November 1999. *J. Geophys. Res.*, **108**(C11), 3370, 10.1029/2003JC001836.
- Kuo, N.-J. and C.-R. Ho (2004): ENSO effect on the sea surface wind and sea surface temperature in the Taiwan Strait. *Geophys. Res. Lett.*, **31**, L13309, doi:10.1029/2004GL020303.
- Li, C., J. Hu, S. Jan, Z. Wei, G. Fang and Q. Zheng (2006): Winter–spring fronts in Taiwan Strait. *J. Geophys. Res.*, **111**, C11S13, doi:10.1029/2005JC003203.

- Liang, W.-D., T. Y. Tang, Y. J. Yang, M. T. Ko and W.-S. Chuang (2003): Upper-ocean currents around Taiwan. *Deep-Sea Res. II*, **50**, 1085–1105.
- Lin, S. F., T. Y. Tang, S. Jan and C.-J. Chen (2005): Taiwan Strait current in winter. *Cont. Shelf Res.*, **25**, 1023–1042.
- Mellor, G. L. and T. Yamada (1982): Development of a turbulence closure model for geophysical fluid problems. *Rev. Geophys. Space Phys.*, **20**, 851–875.
- Milliff, R. F., W. G. Large, J. Morzel, G. Danabasoglu and T. M. Chin (1999): Ocean general circulation model sensitivity to forcing from scatterometer winds. *J. Geophys. Res.*, **104**, 11337–11358.
- Shang, S., C. Zhang, H. Hong, Q. Liu, G. T. F. Wang, C. Hu and B. Huang (2005): Hydrographic and biological changes in the Taiwan Strait during the 1997–1998 El Niño winter. *Geophys. Res. Lett.*, **32**, L11601, doi:10.1029/2005GL022578.
- Smagorinsky, J. (1963): General circulation experiments with the primitive equations. I. The basic experiments. *Mon. Wea. Rev.*, **91**, 99–164.
- Wang, J. and C.-S. Chern (1988): On the Kuroshio branch in the Taiwan Strait during wintertime. *Prog. Oceanogr.*, **21**, 469–491.
- Wang, J. and C.-S. Chern (1992): On the distribution of bottom cold waters in Taiwan Strait during summertime. *La mer*, **30**, 213–221.
- Wu, C.-R. and Y.-C. Hsin (2005): Volume transport through the Taiwan Strait: a numerical study. *Terr., Atmos. Ocean. Sci.*, **16**(2), 377–391.